Topological surface state enhanced ultrafast spin dynamics of Fe/Bi_2Se_3 heterostructures

Na Li,[1,2] Yun-bin Sun,[3] Rui Sun,[1,2] Xu Yang,[1,2] Wei Zhang,[1,2] Zong-kai Xie,[1,2] Jia-nan Liu,[1,2] Yan Li,[1,2] Yang Li,[1,2] Zi-zhao Gong,[1,2] Xiang-qun Zhang,[1] Wei He,[1,*] and Zhao-hua Cheng[1,2,4,†]

[1] *State Key Laboratory of Magnetism and Beijing National Laboratory for Condensed Matter Physics, Institute of Physics, Chinese Academy of Sciences, Beijing 100190, China*

[2] *School of Physical Sciences, University of Chinese Academy of Sciences, Beijing 100049, China*

[3] *Key Laboratory of Magnetism and Magnetic Materials at Universities of Inner Mongolia Autonomous Region, Department of Physics, Baotou Normal University, Baotou 014030, People's Republic of China*

[4] *Songshan Lake Materials Laboratory, Dongguan, Guangdong 523808, China*

(Received 18 October 2021; revised 20 February 2022; accepted 29 March 2022; published 13 April 2022)

Topological insulators (TIs) with distinct topological surface states (TSSs) have served as fertile ground to investigate spintronics and quantum information devices. Spin transport properties of ferromagnet (FM)/TI heterostructures have been revealed due to the spin-momentum-locked TSS. The role of the TSS on laser-induced ultrafast spin dynamics, however, is not well understood. Here, we find that the TSS can not only significantly accelerate the ultrafast demagnetization but can also enhance the Gilbert damping factor of Fe/Bi_2Se_3 heterostructures. We conclude that the TSS enhanced ultrafast spin dynamics is attributed to the strong hybridization of Fe and Bi_2Se_3 orbitals near the Fermi level. Our findings suggest that the manipulation of ultrafast spin dynamics of a FM/TI via the TSS can open an avenue to utilize future topological spintronic devices or quantum information processing approaching femtosecond timescales.

DOI: 10.1103/PhysRevB.105.144415

I. INTRODUCTION

Engineering ultrafast spin dynamics by femtosecond laser pulses, an approach for manipulating spin down to the femtosecond timescale, is an essential task to advance toward the realization of ultrafast spintronic devices [1,2]. The mechanism of ultrafast demagnetization is the most challenging problem in ultrafast spin dynamics [3–5]. The Gilbert damping factor α_G is of utmost importance for high-frequency switching of magnetic devices [6,7]. Although their timescales range from femtoseconds to nanoseconds, both ultrafast demagnetization time τ_M and Gilbert damping factor α_G represent the transfer rate of angular momentum from the electronic system to the lattice.

As a state of quantum matter, topological insulators (TIs) may serve as a platform for both fundamental physics and technological applications such as spintronics and quantum information processing [8,9]. In the case of the prototypical three-dimensional TI Bi_2Se_3, large spin-orbit coupling (SOC) leads to a band inversion in the bulk state and the formation of a topological surface state (TSS) with linear dispersion and helical spin texture [10,11]. The spin-polarized electrons at the TI surface are immune to direct backscattering due to the spin-momentum-locked property and thereby affect the spin transport and spin dynamics in ferromagnet (FM)/TI heterostructures. Consequently, harnessing the TSS in conjunction with magnetic materials will pave the way to realize TI-based spintronic devices. Until recently, the spin Seebeck effect [12], spin-charge conversion [13–15], and spin-orbit torque switching [16,17] in FM/TI heterostructures have been extensively investigated; however, spin dynamics remains elusive. Previous studies suggested that the TSS can modulate the damping factor of the FM layer via ferromagnetic resonance [18,19]; however, its effect on the laser-induced ultrafast demagnetization time τ_M is unknown. As a spin sink layer, the conducting TSS in TIs with spin-momentum-locked helicity texture [10,11] is expected to speed up the quenching and switching of magnetization in FM/TI heterostructures, which may ignite a combining investigation of ultrafast spin dynamics with topological physics and open the field in ultrafast topological spintronics or quantum information processing. Here, we report on laser-induced ultrafast spin dynamics in Fe/Bi_2Se_3 heterostructures. By changing the thickness of Bi_2Se_3 films with and without a TSS, we find that the presence of a TSS can accelerate the ultrafast demagnetization and significantly enhance the Gilbert damping factor. Additionally, *ab initio* electronic structure calculations demonstrate the direct orbital hybridization between the TSS and directly contacted Fe. Our findings can provide further insight into understanding the fundamental and practical limits on the speed of spin manipulation and exploring topological spintronics and quantum information processing technologies on femtosecond timescales.

II. METHODS

High-quality single-crystal Bi_2Se_3 films with thicknesses of 3 and 9 quintuple layers (QL, 1 QL $\approx$ 0.95 nm) were deposited on Si (111) substrate by means of molecular beam epitaxy (see Supplemental Material [20]). To understand the

*hewei@iphy.ac.cn
†zhcheng@iphy.ac.cn

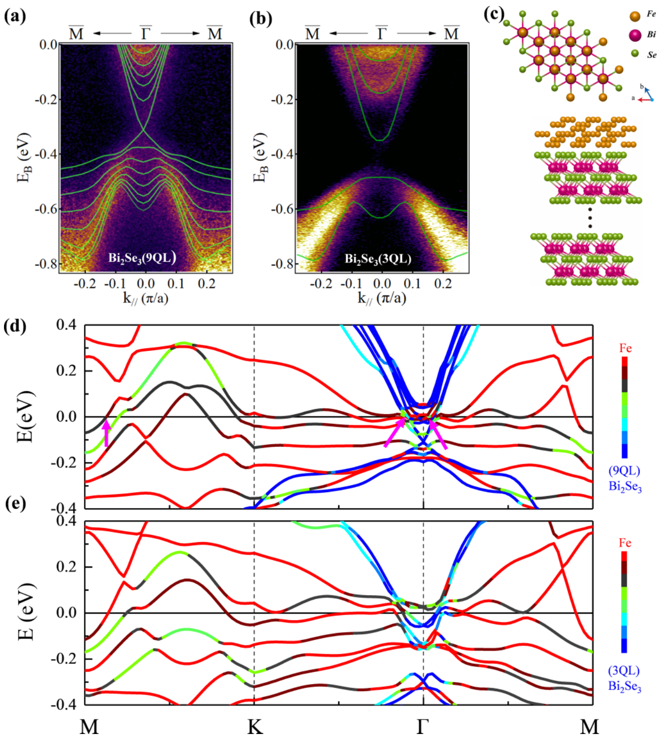

FIG. 1. Electronic band dispersions by angle-resolved photoemission spectroscopy (ARPES) measurement and *ab initio* calculations. (a) Band structure maps of Bi_2Se_3 [9 quintuple layer (QL)] and (b) Bi_2Se_3 (3 QL) by the ARPES (yellow dots) and calculated bands (green lines). (c) Top and side view of atomic arrangement in constructed structure Fe/Bi_2Se_3 for calculations. (d) Calculated band structure of Fe [6 monolayer (ML)]/Bi_2Se_3 (9 QL) and (e) Fe (6 ML)/Bi_2Se_3 (3 QL). In (d) and (e), the color bars indicate spectra weights of Fe and Bi_2Se_3, and the black solid horizontal line denotes Fermi level. The pink arrows in (d) indicate the strong band hybridization between Fe and topological surface state (TSS) of Bi_2Se_3 (9 QL) orbitals near the Fermi level.

thickness dependence of band structure in Bi_2Se_3 film, we perform angle-resolved photoemission spectroscopy (ARPES) measurements, together with *ab initio* electronic structure calculations. Figures 1(a) and 1(b) illustrate the ARPES spectra along the $\overline{M}$-$\overline{\Gamma}$-$\overline{M}$ direction of the first Brillouin zone of Bi_2Se_3 with thickness of 9 and 3 QL, respectively. In addition to bulk bands, 9 QL Bi_2Se_3 contains a perfect linearly dispersing TSS with a well-defined Dirac cone (D_{TI}) at 0.29 eV below the Fermi level. Meanwhile, a bandgap ∼0.10 eV between the bulk conduction band (BCB) and the bulk valance band (BVB) is clearly seen in 3 QL Bi_2Se_3 film [Fig. 1(b)]. Previous work demonstrated that the bandgap originated from the coupling of opposite spin-polarized surfaces by quantum tunneling with Bi_2Se_3 thickness <6QL [21,22].The calculated band structures of Bi_2Se_3 with thicknesses of 9 and 3 QL along $\overline{M}$-$\overline{\Gamma}$-$\overline{M}$, as respectively plotted with green lines in Figs. 1(a) and 1(b), are in good agreement with ARPES results.

The Bi_2Se_3 films with thicknesses of 9 and 3 QL represent two typical band structures, i.e., with or without a TSS. To investigate the effect of band structures on the ultrafast spin dynamics of Fe/Bi_2Se_3, Fe films (11 nm) were deposited on Bi_2Se_3 films with thicknesses of 9 and 3 QL, respectively. It is documented that magnetic doping in Bi_2Se_3 can break the time reversal symmetry, resulting in a gap at the Dirac point [23]. However, previous studies confirmed that the TSS is tolerant against magnetic adsorbates such as Fe with in-plane magnetic anisotropy; namely, TSS still exists, interfacing with an in-plane magnetic anisotropic ferromagnet [24]. For our samples, Fe reveals an in-plane magnetic anisotropy experimentally (see Supplemental Material [20]). Additionally, we calculated the band structure of Fe [6 monolayer (ML)]/Bi_2Se_3 (9 QL) and Fe(6 ML)/Bi_2Se_3(3 QL). *Ab initio* calculations suggest that the Fe layer exhibits an in-plane magnetic anisotropy, consistent with the experiment. Compared with the pristine band structure of Bi_2Se_3, the calculated electronic band of Fe/Bi_2Se_3 (9 QL) in Fig. 1(d) demonstrates that the in-plane magnetic anisotropy of Fe does not significantly alter the topological band structure of Bi_2Se_3, whose TSS is still preserved but hybridizes with Fe orbitals at the Fermi level [Figs. 1(d) and 1(e)]. More clearly, we also extracted the component of the Bi_2Se_3 band from Fe/Bi_2Se_3 (9 QL) (see Supplemental Material [20]). The robustness of the TSS is fortunately the precondition for investigating the ultrafast spin dynamics in FM/TI heterostructures.

To investigate the effect of the TSS on the ultrafast spin dynamics of FM/TI heterostructures, 11-nm-thin Fe films were evaporated on a Bi_2Se_3 surface at room temperature with a surface roughness of ∼0.3 nm (see Supplemental Material [20]). At last, a 3 nm Cu capper with a surface roughness of ∼0.4 nm was evaporated by electron beam for all samples to avoid oxidation. Since the mixed buffer layer $FeSe_x$ at the interface is produced at a relatively high temperature, such as 500 K [25], we deposited the Fe layer at room temperature to exclude the formation of an intermixing buffer layer at interfaces of Bi_2Se_3 and Fe films, by electron beam evaporation. Furthermore, the same values of saturation magnetization of Fe for Fe/Bi_2Se_3 (3 QL), Fe/Bi_2Se_3 (9 QL), and $Fe/Cu/Bi_2Se_3$ (9 QL) imply that no obvious mixed layers change the interface dynamics.

The ultrafast demagnetization curves of Fe/Bi_2Se_3 (3 and 9 QL) were measured by time-resolved magneto-optical Kerr effect (TRMOKE) at room temperature. To separate the contribution from the interfacial coupling between Fe and Bi_2Se_3 on the spin dynamics, 5 nm Cu was inserted between the Fe and Bi_2Se_3 (9 QL). The schematic diagram of these representative samples (without TSS, with TSS, and a Cu inserting layer) and the pump-probe geometry are presented in Figs. 2(a)–2(c). It is a fact that the heat transport affects not only the rate of demagnetization but also the maximum magnetic quenching. In the laser fluence range of 1.0–1.5 mJ/cm^2, the Fe layer reaches a maximum temperature of 315 K calculated by the method in the previous literature [26–33] (see Supplemental Material [20]), which is quite small compared with its Curie temperature T_c (1043 K), indicating that the influence of heat transport on demagnetization time can be neglected. Therefore, we used a fluence of 1.21 mJ/cm^2 to obtain a high enough Kerr signal-to-noise ratio and guarantee that experiments are performed in the linear regime as well. By slightly tuning the pump laser fluence ∼1.21 mJ/cm^2, we can obtain the ultrafast demagnetization curves for various samples with almost the same maximum quenching of ≈5%,

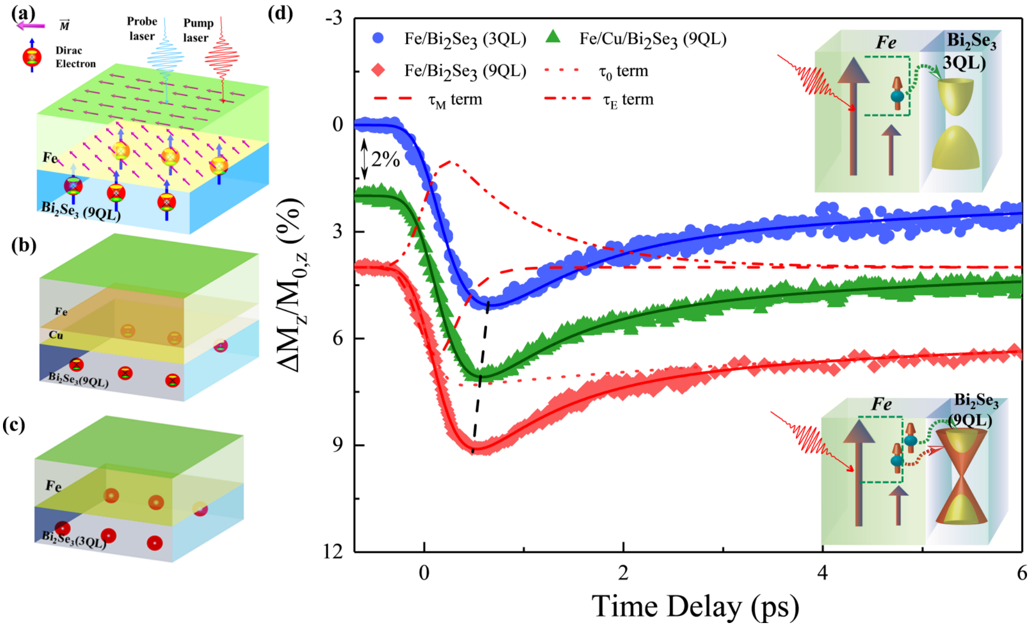

FIG. 2. Schematic diagram of samples and ultrafast demagnetization. Sample configurations of (a) Fe/Bi_2Se_3 [9 quintuple layer (QL)], (b) $Fe/Cu/Bi_2Se_3$ (9 QL), and (c) Fe/Bi_2Se_3 (3 QL). (d) Ultrafast demagnetization curves of different samples, shifted vertically for clarity. The solid lines represent the fitting results by Eq. (1), where the first, second, and third fitting terms are noted by dot, dash, and dash-dot lines for Fe/Bi_2Se_3 (9 QL), respectively. The insets show the excitation and dissipative channel of angular momentum in Bi_2Se_3 with and without topological surface states (TSSs).

as shown in Fig. 2(d). This can ensure the effect of heat transport on all samples is almost the same. A rapid decrease of magnetization takes place on the subpicosecond timescale followed by a pronounced magnetization recovery. The time evolution of magnetization can be fitted by Eq. (1) based on the three-temperature model [34]:

$$-\frac{\Delta M_z(t)}{M_{0,z}} = \left\{\left[\frac{A_1}{(t/\tau_0+1)^{0.5}} - \frac{A_2\tau_E - A_1\tau_M}{\tau_E-\tau_M}\exp\left(-\frac{t}{\tau_M}\right) - \frac{\tau_E(A_1-A_2)}{\tau_E-\tau_M}\exp\left(-\frac{t}{\tau_E}\right)\right]\theta(t) + A_3\delta(t)\right\}G(t,\tau_G), \quad (1)$$

where $G(t, \tau_G)$ represents the convolution product with the Gaussian laser pulse, τ_G is its full width at half maximum (FWHM) with the value of 270 fs in our experiment, $\theta(t)$ is a step function, and $\delta(t)$ is the Dirac function. The constant A_1 represents the value of $-\Delta M_Z/M_{0,Z}$ after the equilibrium between electrons, spins, and lattice is restored; the constant A_2 is proportional to the initial electron temperature rise; and the constant A_3 represents the magnitude of state-filling effects during pump-probe temporal overlap, which can be well described by a delta function. Here, τ_0 represents the cooling time of the whole film by leaser heat diffusion through the substrate. Also, τ_E and τ_M represent the timescale of electron-phonon interactions and the magnetization loss, respectively. Fitted results are shown in solid lines in Fig. 2(d), and then the time parameters are evaluated. Here, τ_0 is about one order of magnitude bigger than τ_E, implying that the heat diffusion and the electron-phonon relaxation processes are not mixed, and consequently, the values obtained for τ_E and τ_M are reliable. We obtained the best fitting with $\tau_E = 870 \pm 10$ fs for the demagnetization curves of all samples. However, the ultrafast demagnetization time presents a completely different character within different samples.

III. RESULTS

Comparing with the value of $\tau_M = 285 \pm 10$ fs for Fe deposited on a conventional insulating MgO substrate (see Supplemental Material [20]), a smaller value of $\tau_M = 255 \pm 10$ fs is observed for Fe/Bi_2Se_3 (3 QL) without the TSS. This difference in ultrafast demagnetization time results from the Fe/MgO and Fe/Bi_2Se_3 interface. MgO is an insulating oxide, while Bi_2Se_3 is a semiconductor with much stronger SOC. The strong SOC facilitates the spin-flip process and reduces demagnetization time. Moreover, although there exists a bandgap of ~0.10 eV between the BCB and the BVB in 3 QL Bi_2Se_3 film, the vacancies of Se in Bi_2Se_3 allow for the BCB to cross the Fermi level [Fig. 1(b)]. The conduction electrons at the Fermi surface of Bi_2Se_3 serve as a channel for spin dissipation and speed up the ultrafast demagnetization process. Meanwhile, there are no conduction electrons at the Fermi surface of a conventional insulating MgO. In the case of coexistence of the TSS and the BCB, the value of τ_M for Fe/Bi_2Se_3 (9 QL) decreases further to 175 ± 10 fs. Since the only difference between 3 and 9 QL Bi_2Se_3 is that the latter contains a TSS, the decrease in the value of τ_M for Fe/Bi_2Se_3 (9 QL) ($\tau_M = 175 \pm 10$ fs) is related to the contribution of the TSS to spin dissipation [inset of Fig. 2(d)].

The TSS of 9 QL Bi_2Se_3 not only serves as an angular momentum dissipation channel by spin-pumping effect but enlarges the interfacial spin-orbital coupling by the magnetic proximity effect (MPE) as well [35–37]. This means the dif-

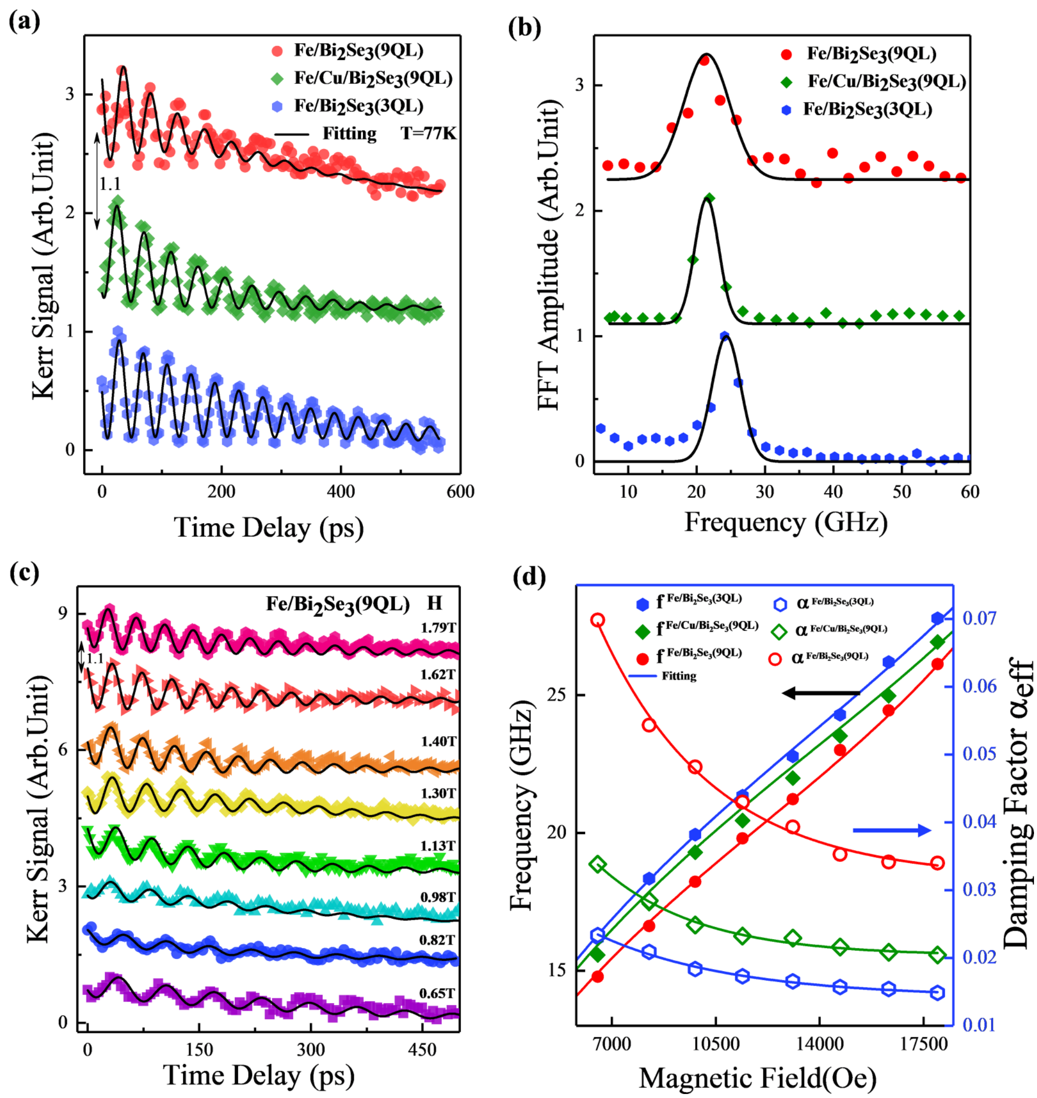

FIG. 3. Typical time-resolved magneto-optical Kerr effect (TRMOKE) results and magnetic-field-related frequency and damping factor of Fe/Cu (0 and 5 nm)/Bi_2Se_3 [3 and 9 quintuple layer (QL)] at 77 K. (a) TRMOKE results of the samples at $T = 77$ K under 10 kOe and (b) their corresponding fast Fourier transform (FFT) results. (c) TRMOKE signals for Fe/Bi_2Se_3 (9 QL) under various fields at 77 K. The solid lines are the fitting results by Eq. (2) in (a) and (c) and the Gaussian fitting in (b) where the vertical values are offset for clarity. (d) Field dependence of frequency (left) and damping factors (right) of the three samples at 77 K. The solid lines are fitting results by Eqs. (3) and (4), respectively.

ference in ultrafast demagnetization time of ~80 fs between Fe/Bi_2Se_3 (9 QL) and Fe/Bi_2Se_3 (3 QL) is attributed to both the spin-pumping effect and the MPE. Since the deposition of Cu on Bi_2Se_3 does not destroy the TSS [38] and the spin diffusion length of Cu is ~50 nm [39], a 5 nm Cu layer inserted between Fe and Bi_2Se_3 (9 QL) can exclude the MPE without losing the spin-pumping effect. The ultrafast demagnetization time decreases from 255 ± 10 fs for Fe/Bi_2Se_3 (3 QL) to 200 ± 10 fs for (9 QL) with introducing the TSS and further decreases to 175 ± 10 fs for Fe/Bi_2Se_3 (9 QL) with introducing the MPE.

Considering the same bulk SOC and interfacial geometry between Fe/Bi_2Se_3 (3 QL) and Fe/Bi_2Se_3 (9 QL), the large difference in ultrafast demagnetization time is attributed to the difference in the band structures of Bi_2Se_3 with various thicknesses. From Figs. 1(d) and 1(e), in addition to the existence of the TSS, we find strong band hybridization between Fe and the TSS of Bi_2Se_3 (9 QL) orbitals around the $\bar{\Gamma}$ point near the Fermi level [see pink arrows marked in Fig. 1(d)]. The topological nature of Bi_2Se_3 (9 QL) facilitates this hybridization and results in more hybridized states around the Fermi level, accelerating the ultrafast demagnetization.

In addition to faster magnetization quenching, the TSS can enhance the damping factor on a subnanosecond timescale. To fully understand the TSS-modulated spin dynamics, magnetization precession measurements were conducted from 77 to 300 K. Figure 3(a) shows the typical magnetic precession of Fe/Bi_2Se_3 (3 QL), Fe/Bi_2Se_3 (9 QL), and Fe/Cu/Bi_2Se_3 (9 QL) films under a magnetic field of 10 kOe at 77 K. Obviously, the oscillation amplitude for the Fe/Bi_2Se_3 (9 QL) film undergoes a noticeable attenuation with increasing time delay, which indicates the magnetization relaxation is faster compared with slow relaxation by inserting a Cu layer. The Fe/Bi_2Se_3 (3 QL) film does not decay significantly in the range of 1 ns. Moreover, the FWHM of fast Fourier transform (FFT) spectra for the Fe/Bi_2Se_3 (9 QL) film is nearly twice as wide than that for the Fe/Bi_2Se_3 (3 QL) film [Fig. 3(b)]. All of these demonstrate that Fe/Bi_2Se_3 (9QL) possesses the largest damping factor. Additionally, the distinct shift of the FFT peaks between Fe/Bi_2Se_3 (3 QL) and Fe/Bi_2Se_3 (9 QL) samples indicates the precession frequency is also modulated by the TSS. The TRMOKE signals can be fitted by Eq. (2) [40]:

$$\theta_\kappa = A + Be^{-\upsilon t} + C\exp\left(-\frac{t}{\tau}\right)\sin(2\pi ft + \varphi), \quad (2)$$

where C, τ, f, φ are magnetization precession amplitude, relaxation time, frequency, and phase, respectively, and A, B, and υ correspond to background signal from the slow recovery process. From the best-fitted curves, the precession frequency f and relaxation time τ can be extracted. To deeply uncover the effect of the TSS on the dynamic parameters of the Fe layer, magnetic-field-dependent TRMOKE was performed with typical curves of Fe/Bi_2Se_3 (9 QL) presented in Fig. 3(c). The experimental $f-H$ relation is generally described by Kittel Eq. (3) [41]:

$$\begin{aligned} f &= \frac{\gamma}{2\pi M_s \sin\theta}\sqrt{(H_a H_b)}, \\ H_a &= 2K_u\cos2\theta + 2K_{\rm int}\cos2\theta + \mu_0 H M_s\cos(\theta-\theta_H) \\ &\quad - \mu_0 M_s^2\cos2\theta - (K_u\sin2\theta)^2, \\ H_b &= 2K_u\sin^2\theta + \mu_0 H M_s\sin\theta_H, \end{aligned} \quad (3)$$

where K_u and $K_{\rm int}$ are the uniaxial magnetic anisotropy constant and the interfacial magnetic anisotropy constant induced by Bi_2Se_3 [19], respectively. Here, M_s is the saturation magnetization of Fe obtained from the M-H curve via superconducting quantum interference device (see Supplemental Material [20]). Also, γ and μ_0 are the gyromagnetic ratio and vacuum permeability, respectively. The equilibrium angular position θ of the magnetization is satisfied by the equation: $\sin2\theta = (2H\mu_0/H_K)\sin(\theta-\theta_H)$, $H_K = \frac{2(K_u-K_{\rm int})}{M_s} + \mu_0 M_s$. The direction of applied field is kept as $\theta_H = 9.5^\circ$. Furthermore, we can calculate the effective damping factor with Eq. (4) [41]:

$$\alpha_{\rm eff} = \frac{2}{\gamma\tau\left(H_a + \frac{H_b}{\sin^2\Theta_M}\right)}. \quad (4)$$

Figure 3(d) presents the dependence of f and effective damping factor $\alpha_{\rm eff}$ under different magnetic field at 77 K, well fitted separately using Eqs. (3) and (4). A shift of f of 2 GHz between Fe/Bi_2Se_3 (3 QL) and Fe/Bi_2Se_3 (9 QL) implies that the magnetic anisotropy constants can be modified by the TSS. In addition, the $\alpha_{\rm eff}$ of the Fe/Bi_2Se_3 (9 QL) sample with a gapless TSS is two times larger than that of the Fe/Bi_2Se_3 (3 QL) sample at the same magnetic field.

The effective damping factor $\alpha_{\rm eff}$ consists of intrinsic Gilbert-type damping and extrinsic contribution. The latter is originated from both the two-magnon scattering and dephasing effect and can be excluded via a higher applied field. Figure 3(d) shows the effective damping factor decreases monotonously to a constant value with increasing field. Thus, the Gilbert-type damping factor can be obtained by fitting the field dependent $\alpha_{\rm eff}$ using Eq. (5) [42,43]:

$$\alpha_{\rm eff} = \alpha_{\rm G} + \alpha_1\exp\left(-\frac{H}{H_0}\right). \quad (5)$$

Figures 4(a) and 4(b) show the temperature-dependent f and Gilbert-type damping factor $\alpha_{\rm G}$, respectively. For the Fe/Bi_2Se_3 (3 QL) sample, both f and $\alpha_{\rm G}$ remain almost unchanged in the whole temperature region. On the contrary, for the Fe/Bi_2Se_3 (9 QL) sample, f increases, and $\alpha_{\rm G}$ decreases significantly with increasing temperature from 77 to 150 K, and both are nearly constant with increasing temperature. Therefore, we can conclude that the TSS of 9 QL Bi_2Se_3 strongly affects the dynamic parameters. Like the change of ultrafast demagnetization time, the enhancement of Gilbert-type damping in Fe/Bi_2Se_3 (9 QL) also originates from the spin-pumping effect [15] (nonlocal) and the MPE (local). As for the spin-pumping effect, the spin-momentum-locked TSS has been thought of as the most efficient angular momentum dissipating channel exceeding the performance of heavy metals [15,44]. When the TSS of Bi_2Se_3 was decoupled with Fe by Cu, both the precession frequency and Gilbert damping factor of Fe/Bi_2Se_3 (9 QL) sustain a quite similar trend in the whole temperature region. By comparing the values of the damping factor of $Fe/Cu/Bi_2Se_3$ (9 QL) with those of Fe/Bi_2Se_3 (3 QL), the contribution of the spin-pumping effect from TSS can be derived. Considering the role of spin-dependent interface transparency, the spin-pumping effect is more significant. Our results provide the lower bound of its contribution. The nonlocal angular momentum dissipation at the interface opens an additional channel to accelerate the ultrafast demagnetization and enhance the Gilbert damping. In our previous work, we also found the ultrafast demagnetization time decreases with increasing Gilbert damping induced by the angular momentum in $Fe_{81}Ga_{19}/IrMn$ bilayers [45].

After excluding the spin-pumping effect, the additional enhancement of the damping factor of Fe/Bi_2Se_3 (9 QL) is ascribed to the strong interfacial coupling between the Fe layer and the Bi_2Se_3 (9 QL) layer with the TSS.

Therefore, the overall Gilbert-type damping factor of Fe/Bi_2Se_3 (9 QL) can be written as

$$\alpha_{\rm G}^{\rm Fe/Bi_2Se_3(9QL)} = \alpha_{\rm G}^{\rm Fe/Bi_2Se_3(3QL)} + \alpha_{\rm SP} + \alpha_{\rm MPE}, \quad (6)$$

where $\alpha_{\rm SP}$ and $\alpha_{\rm MPE}$ are the damping factors due to the spin-pumping effect and the MPE, respectively.

In the presence of interfacial SOC strength ξ from the MPE, $\alpha_{\rm MPE}$ can be simply expressed as [46–48]

$$\alpha_{\rm MPE} \sim \frac{D(E_{\rm F})\xi^2\tau^{-1}}{M_s}, \quad (7)$$

where $D(E_{\rm F})$ is the density of states at the Fermi level, ξ is the strength of SOC, and τ^{-1} is the electron scattering rate.

To understand the temperature dependence of the Gilbert damping factor of Fe/Bi_2Se_3 (9 QL), one should consider the interfacial SOC. According to the Kittel equation, the temperature dependence of the magnetic anisotropy constants of $K_{\rm int}$ and K_u for the three samples were obtained by Eq. (3) and plotted in Fig. 4(c). The value of $K_{\rm int}$ for Fe/Bi_2Se_3 (9 QL) is as high as 10^5 J/m^3, two orders of magnitude larger than that

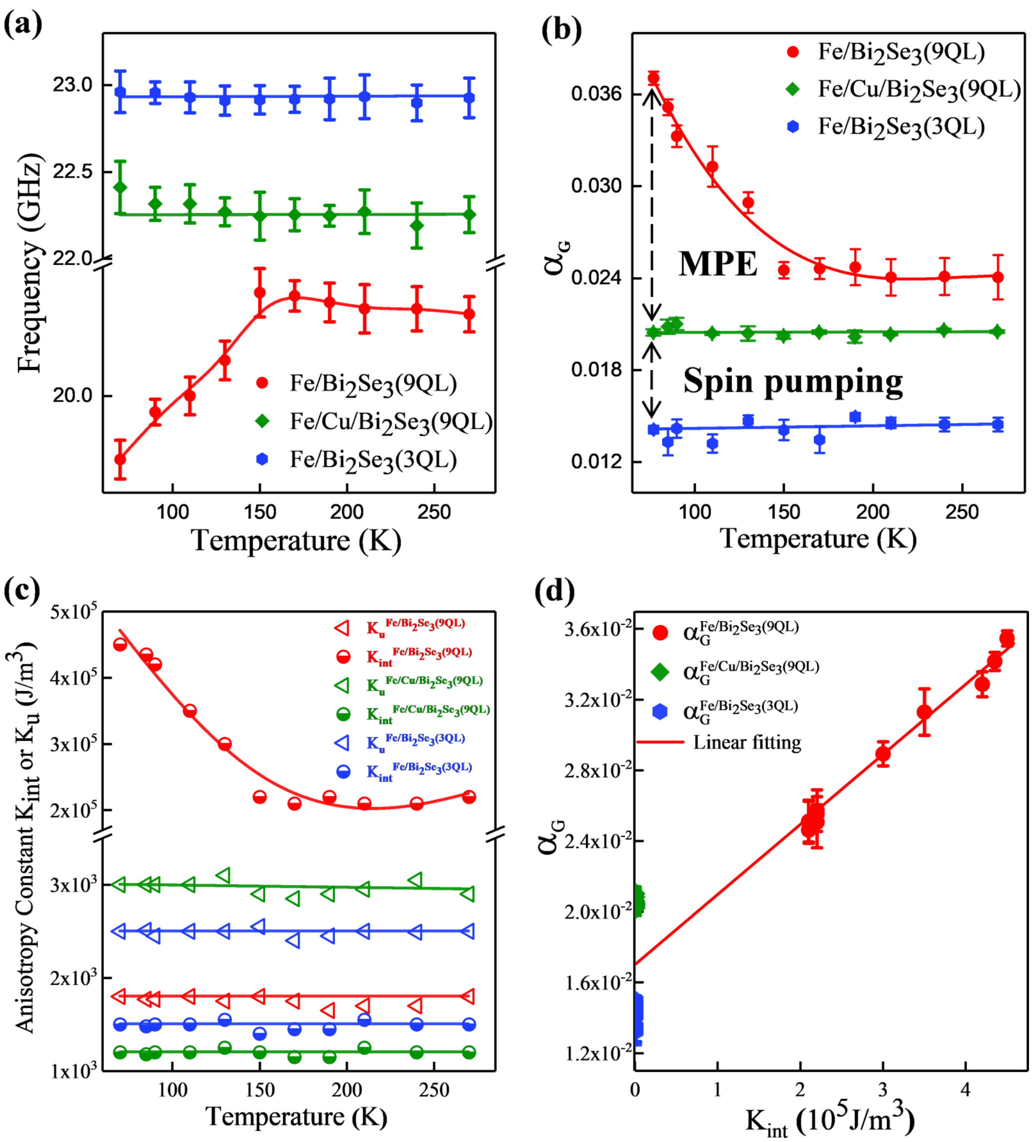

FIG. 4. Temperature dependence of dynamic characteristics. (a) Temperature dependence of frequency, (b) Gilbert damping factor, and (c) uniaxial anisotropy constant as well as interfacial anisotropy constant. The solid lines are a guide for eyes. (d) Relationship between Gilbert damping factor and interfacial anisotropy constant; the solid line is the linear fitting result.

in the other two samples, suggesting that the orbital hybridization strongly enhances the interfacial SOC for Fe/Bi_2Se_3 (9 QL) bilayer. With increasing temperature from 77 to 150 K, a dramatic decrease in K_{int} of Fe/Bi_2Se_3 (9 QL) is observed, while K_{int} of Fe/Bi_2Se_3 (3 QL) and $Fe/Cu/Bi_2Se_3$ (9 QL) are almost identical. The interfacial magnetic anisotropy was modified by direct contact with the TSS of Bi_2Se_3 and substantially modulated the precession frequency and damping factor of the Fe layer.

The temperature-dependent magnetic anisotropy, precession frequency, and Gilbert damping originate from proximate exchange coupling (SOC-induced anisotropies) between Fe and Bi_2Se_3. The possible reasons for the strong temperature dependence $<150\,K$ are the relatively weak exchange coupling between Fe and the TSS of Bi_2Se_3. This weak exchange coupling would compete with the thermal fluctuations. The turning point at low temperature such as 150 K is expected where weak exchange coupling can overcome the thermal fluctuations. The weak exchange coupling shows a strong temperature dependence of the anisotropy, precession frequency, and Gilbert damping at low temperatures. Similar transitions in FM/TI were also reported in Bi_2Se_3/magnetic materials, such as yttrium iron garnet [49–51]. The strong temperature-dependent effect $<150\,\mathrm{K}$ probably results from the relatively enhanced exchange coupling associated with increased conductivity of the TSS in Bi_2Se_3 at low temperature. Since K_{int} is also dominated by the interfacial SOC ξ, a rough estimate of K_{int} can be written as [52]

$$K_{\mathrm{int}} \sim \frac{\xi^2}{W}, \tag{8}$$

where W is the bandwidth of d electrons.

If we approximately assume that the density of states $D(E_{\mathrm{F}})$, scattering time τ, saturation magnetization M_s, and the bandwidth of d electrons W vary slightly in the measured temperature region, α_{MPE} should be proportional to K_{int} by combining Eqs. (7) and (8). As shown in Fig. 4(d), α_G increases linearly with K_{int} for Fe/Bi_2Se_3 (9 QL), suggesting that the enhanced Gilbert-type damping factor mostly originates from interfacial SOC at Fe/Bi_2Se_3 (9 QL). When we extrapolate the value of K_{int} to zero, the value of α_G is comparable with those of Fe/Bi_2Se_3 (3 QL) and $Fe/Cu/Bi_2Se_3$ (9 QL). Again, considering the band structures observed in Fig. 1(d), the additional damping factor of Fe/Bi_2Se_3 (9 QL) is ascribed to the strong band hybridization of Fe and Bi_2Se_3 orbitals at the Fermi level. Based on the scattering theory of Gilbert damping, Hou and Wu [46] calculated that the Gilbert damping is strongly enhanced by about one order of magnitude compared with damping of their bulk forms. The TSS can facilitate the hybridization between Fe and Bi_2Se_3 orbitals and enlarge the interfacial magnetic anisotropy and hence speed up the demagnetization and enhance the Gilbert damping factor.

IV. CONCLUSIONS

We have investigated laser-induced ultrafast spin dynamics in Fe/Bi_2Se_3 heterostructures by tuning band structures of Bi_2Se_3. We find that the existence of the TSS significantly accelerates the ultrafast demagnetization and enhances the Gilbert damping factor. Based on the TRMOKE results and first-principles electronic structure calculations, we conclude that the TSS enhanced ultrafast spin dynamics is attributed to the strong hybridization of Fe and Bi_2Se_3 orbitals near the Fermi level. In this paper, we not only reveal the mechanism of multiple angular momentum dissipation channels in Fe/Bi_2Se_3 but open an avenue to utilize FM/TI topological spintronic devices approaching femtosecond timescales as well.

ACKNOWLEDGMENTS

This paper is supported by the National Natural Sciences Foundation of China (Grants No. 52031015, No. 1187411, No. 51427801, and No. 51871235), the National Key Research Program of China (Grants No. 2016YFA0300701, No. 2017YFB0702702, and No. 2018YFF01010303), and the Key Research Program of Frontier Sciences, CAS (Grants No. QYZDJ-SSW-JSC023, No. KJZD-SW-M01, and No. ZDYZ2012-2).

[1] A. Kirilyuk, A. V. Kimel, and T. Rasing, Ultrafast optical manipulation of magnetic order, Rev. Mod. Phys. **82**, 2731 (2010).

[2] T. Seifert, S. Jaiswal, U. Martens, J. Hannegan, L. Braun, P. Maldonado, F. Freimuth, A. Kronenberg, J. Henrizi, I. Radu, E. Beaurepaire, Y. Mokrousov, P. M. Oppeneer, M. Jourdan, G. Jakob, D. Turchinovich, L. M. Hayden, M. Wolf, M. Münzenberg, M. Kläui *et al.*, Efficient metallic spintronic emitters of ultrabroadband terahertz radiation, Nat. Photonics **10**, 483 (2016).

[3] B. Koopmans, G. Malinowski, F. Dalla Longa, D. Steiauf, M. Fähnle, T. Roth, M. Cinchetti, and M. Aeschlimann, Explaining the paradoxical diversity of ultrafast laser-induced demagnetization, Nat. Mater. **9**, 259 (2010).

[4] J.-Y. Bigot, M. Vomir, and E. Beaurepaire, Coherent ultrafast magnetism induced by femtosecond laser pulses, Nat. Phys. **5**, 515 (2009).

[5] V. Unikandanunni, R. Medapalli, E. E. Fullerton, K. Carva, P. M. Oppeneer, and S. Bonetti, Anisotropic ultrafast spin dynamics in epitaxial cobalt, Appl. Phys. Lett. **118**, 232404 (2021).

[6] I. Zutic, J. Fabian, and S. D. Sarm, Spintronics fundamentals and applications, Rev. Mod. Phys. **76**, 323 (2004).

[7] D. C. Ralph and M. D. Stiles, Spin transfer torques, J. Magn. Magn. Mater. **320**, 1190 (2008).

[8] X. L. Qi, R. Li, J. Zang, and S. C. Zhang, Inducing a magnetic monopole with topological surface states, Science **323**, 1184 (2009).

[9] R. Yu, W. Zhang, H.-J. Zhang, S.-C. Zhang, X. Dai, and Z. Fang, Quantized anomalous Hall effect in magnetic topological insulators, Science **329**, 61 (2010).

[10] D. Hsieh, Y. Xia, D. Qian, L. Wray, J. H. Dil, F. Meier, J. Osterwalder, L. Patthey, J. G. Checkelsky, N. P. Ong, A. V. Fedorov, H. Lin, A. Bansil, D. Grauer, Y. S. Hor, R. J. Cava, and M. Z. Hasan, A tunable topological insulator in the spin helical Dirac transport regime, Nature (London) **460**, 1101 (2009).

[11] S. Y. Xu, Y. Xia, L. A. Wray, S. Jia, F. Meier, J. H. Dil, J. Osterwalder, B. Slomski, A. Bansil, H. Lin, R. J. Cava, and M. Z. Hasan, Topological phase transition and texture inversion in a tunable topological insulator, Science **332**, 560 (2011).

[12] Z. Jiang, C. Z. Chang, M. R. Masir, C. Tang, Y. Xu, J. S. Moodera, A. H. MacDonald, and J. Shi, Enhanced spin Seebeck effect signal due to spin-momentum locked topological surface states, Nat. Commun. **7**, 11458 (2016).

[13] Y. Shiomi, K. Nomura, Y. Kajiwara, K. Eto, M. Novak, K. Segawa, Y. Ando, and E. Saitoh, Spin-electricity Conversion Induced by Spin Injection into Topological Insulators, Phys. Rev. Lett. **113**, 196601 (2014).

[14] K. Kondou, R. Yoshimi, A. Tsukazaki, Y. Fukuma, J. Matsuno, K. S. Takahashi, M. Kawasaki, Y. Tokura, and Y. Otani, Fermi-level-dependent charge-to-spin current conversion by Dirac surface states of topological insulators, Nat. Phys. **12**, 1027 (2016).

[15] R. Sun, S. Yang, X. Yang, E. Vetter, D. Sun, N. Li, L. Su, Y. Li, Y. Li, Z. Z. Gong, Z. K. Xie, K. Y. Hou, Q. Gul, W. He, X. Q. Zhang, and Z. H. Cheng, Large tunable spin-to-charge conversion induced by hybrid Rashba and Dirac surface states in topological insulator heterostructures, Nano. Lett. **19**, 4420 (2019).

[16] Y. Fan, P. Upadhyaya, X. Kou, M. Lang, S. Takei, Z. Wang, J. Tang, L. He, L. T. Chang, M. Montazeri, G. Yu, W. Jiang, T. Nie, R. N. Schwartz, Y. Tserkovnyak, and K. L. Wang, Magnetization switching through giant spin-orbit torque in a magnetically doped topological insulator heterostructure, Nat. Mater. **13**, 699 (2014).

[17] A. Mellnik, J. Lee, A. Richardella, J. Grab, P. Mintun, M. H. Fischer, A. Vaezi, A. Manchon, E.-A. Kim, and N. Samarth, Spin-transfer torque generated by a topological insulator, Nature (London) **511**, 449 (2014).

[18] Q. S. C.Tang, C. Chang, Y. Xu, Y. Ohnuma, M. Matsuo, Y. Liu, W. Yuan, Y. Yao, J. S. Moodera, S. Maekawa, W. Han, and J. Shi, Dirac surface state–modulated spin dynamics in a ferrimagnetic insulator at room temperature, Sci. Adv. **4**, eaas8660 (2018).

[19] Y. T. Fanchiang, K. H. M. Chen, C. C. Tseng, C. C. Chen, C. K. Cheng, S. R. Yang, C. N. Wu, S. F. Lee, M. Hong, and J. Kwo, Strongly exchange-coupled and surface-state-modulated magnetization dynamics in Bi_2Se_3/yttrium iron garnet heterostructures, Nat. Commun. **9**, 223 (2018).

[20] See Supplemental Material at http://link.aps.org/supplemental/10.1103/PhysRevB.105.144415 for details of sample growth, ultrafast measurement, band measurement and calculation, and the laser heating effect on demagnetization.

[21] C.-X. Liu, H. Zhang, B. Yan, X.-L. Qi, T. Frauenheim, X. Dai, Z. Fang, and S.-C. Zhang, Oscillatory crossover from two-dimensional to three-dimensional topological insulators, Phys. Rev. B **81**, 041307(R) (2010).

[22] Y. Zhang, K. He, C. Z. Chang, C. L. Song, L. L. Wang, X. Chen, J. F. Jia, Z. Fang, X. Dai, W.-Y. Shan, S.-Q. Shen, Q. Niu, X.-L. Qi, S.-C. Zhang, X.-C. Ma, and Q.-K. Xue, Crossover of the three-dimensional topological insulator Bi_2Se_3 to the two-dimensional limit, Nat. Phys. **6**, 584 (2010).

[23] Y. L. Chen, J.-H. Chu, J. G. Analytis, Z. K. Liu, K. Igarashi, H.-H. Kuo, X. L. Qi, S. K. Mo, R. G. Moore, D. H. Lu, M. Hashimoto, T. Sasagawa, S. C. Zhang, I. R. Fisher, Z. Hussain, and Z. X. Shen, Massive Dirac fermion on the surface of a magnetically doped topological insulator, Science **329**, 659 (2010).

[24] J. Honolka, A. A. Khajetoorians, V. Sessi, T. O. Wehling, S. Stepanow, J.-L. Mi, B. B. Iversen, T. Schlenk, J. Wiebe, N. B. Brookes, A. I. Lichtenstein, P. Hofmann, K. Kern, and R. Wiesendanger, In-plane Magnetic Anisotropy of Fe Atoms on Bi_2Se_3(111), Phys. Rev. Lett. **108**, 256811 (2012).

[25] A. Polyakov, H. L. Meyerheim, E. D. Crozier, R. A. Gordon, K. Mohseni, S. Roy, A. Ernst, M. G. Vergniory, X. Zubizarreta, M. M. Otrokov, E. V. Chulkov, and J. Kirschner, Surface alloying and iron selenide formation in $Fe/Bi_2Se_3(0001)$ observed by x-ray absorption fine structure experiments, Phys. Rev. B **92**, 045423 (2015).

[26] A. J. Schellekens, K. C. Kuiper, R. R. de Wit, and B. Koopmans, Ultrafast spin-transfer torque driven by femtosecond pulsed-laser excitation, Nat. Commun. **5**, 4333 (2014).

[27] L. Le Guyader, A. Kleibert, F. Nolting, L. Joly, P. M. Derlet, R. V. Pisarev, A. Kirilyuk, T. Rasing, and A. V. Kimel, Dynamics of laser-induced spin reorientation in $Co/SmFeO_3$ heterostructure, Phys. Rev. B **87**, 054437 (2013).

[28] K. Ohta and H. Ishida, Matrix formalism for calculation of electric field intensity of light in stratified multilayered films, Appl. Opt. **29**, 1952 (1990).

[29] J. Tang, Y. Ke, W. He, X. Zhang, W. Zhang, N. Li, Y. Zhang, Y. Li, and Z. Cheng, Ultrafast photoinduced multimode antiferromagnetic spin dynamics in exchange-coupled $Fe/RFeO_3$ ($R = \mathrm{Er}$ or Dy) heterostructures, Adv. Mater. **30**, e1706439 (2018).

[30] P. B. Johnson and R. W. Christy, Optical constants of the noble metals, Phys. Rev. B **6**, 4370 (1972).

[31] P. Johnson and R. Christy, Optical constants of transition metals: Ti, V, Cr, Mn, Fe, Co, Ni, and Pd, Phys. Rev. B **9**, 5056 (1974).

[32] J. Yao, K. J. Koski, W. Luo, J. J. Cha, L. Hu, D. Kong, V. K. Narasimhan, K. Huo, and Y. Cui, Optical transmission enhancement through chemically tuned two-dimensional bismuth chalcogenide nanoplates, Nat. Commun. **5**, 5670 (2014).

[33] R. Sultana, G. Awana, B. Pal, P. K. Maheshwari, M. Mishra, G. Gupta, A. Gupta, S. Thirupathaiah, and V. P. S. Awana, Electrical, thermal and spectroscopic characterization of bulk Bi_2Se_3 topological insulator, J. Supercond. Nov. Magn. **30**, 2031 (2017).

[34] G. Malinowski, F. D. Longa, J. H. H. Rietjens, P. V. Paluskar, R. Huijink, H. J. M. Swagten, and B. Koopmans, Control of speed and efficiency of ultrafast demagnetization by direct transfer of spin angular momentum, Nat. Phys. **4**, 855 (2008).

[35] F. Katmis, V. Lauter, F. S. Nogueira, B. A. Assaf, M. E. Jamer, P. Wei, B. Satpati, J. W. Freeland, I. Eremin, D. Heiman, P. Jarillo-Herrero, and J. S. Moodera, A high-temperature ferromagnetic topological insulating phase by proximity coupling, Nature (London) **533**, 513 (2016).

[36] M. Lang, M. Montazeri, M. C. Onbasli, X. Kou, Y. Fan, P. Upadhyaya, K. Yao, F. Liu, Y. Jiang, W. Jiang, K. L. Wong, G. Yu, J. Tang, T. Nie, L. He, R. N. Schwartz, Y. Wang, C. A. Ross, and K. L. Wang, Proximity induced high-temperature magnetic order in topological insulator–ferrimagnetic insulator heterostructure, Nano Lett. **14**, 3459 (2014).

[37] G. Z. C. Tang, Y. Liu, Z. Jiang, C. Liu, M. R. McCartney, D. J. Smith, T. Chen, J. S. Moodera, and J. Shi, Above 400-K robust perpendicular ferromagnetic phase in a topological insulator, Sci. Adv **3**, e1700307 (2017).

[38] J. M. Marmolejo-Tejada, K. Dolui, P. Lazic, P. H. Chang, S. Smidstrup, D. Stradi, K. Stokbro, and B. K. Nikolic, Proximity band structure and spin textures on both sides of topological-insulator/ferromagnetic-metal interface and their charge transport probes, Nano. Lett. **17**, 5626 (2017).

[39] S. Yakata, Y. Ando, T. Miyazaki, and S. Mizukami, Temperature dependences of spin-diffusion lengths of Cu and Ru layers, Jpn. J. Appl. Phys. **45**, 3892 (2006).

[40] M. van Kampen, C. Jozsa, J. T. Kohlhepp, P. LeClair, L. Lagae, W. J. M. de Jonge, and B. Koopmans, All-Optical Probe of Coherent Spin Waves, Phys. Rev. Lett. **88**, 227201 (2002).

[41] G. M. Müller, M. Münzenberg, G. X. Miao, and A. Gupta, Activation of additional energy dissipation processes in the magnetization dynamics of epitaxial chromium dioxide films, Phys. Rev. B **77**, 020412(R) (2008).

[42] X. Ma, L. Ma, P. He, H. B. Zhao, S. M. Zhou, and G. Lüpke, Role of antisite disorder on intrinsic Gilbert damping in L_{10}FePt films, Phys. Rev. B **91**, 014438 (2015).

[43] W. Zhang, W. He, X.-Q. Zhang, Z.-H. Cheng, J. Teng, and M. Fähnle, Unifying ultrafast demagnetization and intrinsic Gilbert damping in Co/Ni bilayers with electronic relaxation near the Fermi surface, Phys. Rev. B **96**, 220415(R) (2017).

[44] Y. Ando and M. Shiraishi, Spin to charge interconversion phenomena in the interface and surface states, J. Phys. Soc. Jpn. **86**, 011001 (2017).

[45] W. Zhang, Q. Liu, Z. Yuan, K. Xia, W. He, Q.-f. Zhan, X. q. Zhang, and Z. h. Cheng, Enhancement of ultrafast demagnetization rate and Gilbert damping driven by femtosecond laser-induced spin currents in $Fe_{81}Ga_{19}/Ir_{20}Mn_{80}$ bilayers, Phys. Rev. B **100**, 104412 (2019).

[46] Y. S. Hou and R. Q. Wu, Strongly Enhanced Gilbert Damping in 3*d* Transition-Metal Ferromagnet Monolayers in Contact with the Topological Insulator Bi_2Se_3, Phys. Rev. Applied **11**, 054032 (2019).

[47] I. Garate and A. MacDonald, Gilbert damping in conducting ferromagnets. II. Model tests of the torque-correlation formula, Phys. Rev. B **79**, 064404 (2009).

[48] S. Mizukami, F. Wu, A. Sakuma, J. Walowski, D. Watanabe, T. Kubota, X. Zhang, H. Naganuma, M. Oogane, Y. Ando, and T. Miyazaki, Long-Lived Ultrafast Spin Precession in Manganese Alloys Films with a Large Perpendicular Magnetic Anisotropy, Phys. Rev. Lett. **106**, 117201 (2011).

[49] X. Che, K. Murata, L. Pan, Q. L. He, G. Yu, Q. Shao, G. Yin, P. Deng, Y. Fan, B. Ma, X. Liang, B. Zhang, X. Han, L. Bi, Q. H. Yang, H. Zhang, and K. L. Wang, Proximity-induced magnetic order in a transferred topological insulator thin film on a magnetic insulator, ACS Nano **12**, 5042 (2018).

[50] S. Zhu, D. Meng, G. Liang, G. Shi, P. Zhao, P. Cheng, Y. Li, X. Zhai, Y. Lu, L. Chen, and K. Wu, Proximity-induced magnetism and an anomalous Hall effect in $Bi_2Se_3/LaCoO_3$: A topological insulator/ferromagnetic insulator thin film heterostructure, Nanoscale **10**, 10041 (2018).

[51] P. Wei, F. Katmis, B. A. Assaf, H. Steinberg, P. Jarillo-Herrero, D. Heiman, and J. S. Moodera, Exchange-Coupling-Induced Symmetry Breaking in Topological Insulators, Phys. Rev. Lett. **110**, 186807 (2013).

[52] P. Bruno, Tight-binding approach to the orbital magnetic moment and magnetocrystalline anisotropy of transition-metal monolayers, Phys. Rev. B **39**, 865 (1989).